doi.org/10.36721/PJPS.2026.39.12.348.1

Albiflorin suppresses breast cancer via the HINT2/NLRP3 signaling pathway

Yunpeng Hu, Chen Li and Yiyao Cui*
Department of Thyroid and Breast Surgery, The Affiliated Jiangning Hospital of Nanjing Medical University, Nanjing, China

Abstract: **Background**: Breast cancer (BC) remains a significant global health threat with complex pathogenesis often linked to chemotherapy resistance and inflammatory microenvironments. Histidine triad nucleotide-binding protein 2 (HINT2) is a mitochondrial protein involved in metabolism and immunity, but its specific role in BC and potential as a therapeutic target require further elucidation. **Objectives**: This study aimed to identify novel therapeutic targets for BC and evaluate the anti-tumor efficacy and molecular mechanisms of Albiflorin (Al), a natural monoterpene glycoside. **Methods**: Proteomic profiling was performed on BC xenografts in nude mice to identify differentially expressed proteins. *In-vivo* and *in-vitro* models (MDA-MB-231 cells) were established to assess the effects of Al (20 mg/kg or 20 μM) on tumor growth, apoptosis and cytokine production. Molecular docking and co-immunoprecipitation (Co-IP) were used to investigate the interactions among HINT2, NLRP3 and Al. **Results**: HINT2 was significantly upregulated in BC tissues and identified as a primary pro-tumorigenic factor. Co-IP confirmed an endogenous interaction between HINT2 and NLRP3. Al exhibited strong binding affinity to HINT2 (–7.36 kcal/mol) and significantly suppressed tumor volume and weight. Furthermore, Al treatment downregulated the HINT2/NLRP3 axis, reduced inflammatory cytokines (IL-1β, IL-6, TNF-α) and promoted apoptosis by modulating Caspase-3, Bax and Bcl-2 levels. **Conclusion**: Albiflorin suppresses BC progression by inhibiting the HINT2/NLRP3 signaling pathway, suggesting HINT2 is a viable biomarker and Al a promising therapeutic agent for BC treatment.

Keywords: Breast cancer; HINT2; NLRP3

Submitted on 17-07-2025 – Revised on 12-09-2025 – Accepted on 20-09-2025

INTRODUCTION

Breast cancer (BC) accounts for approximately 1.7 million new cases worldwide, posing a serious threat to women's physical and psychological well-being. In recent years, advancements in early screening and the standardization of diagnostic and therapeutic approaches, including chemotherapy, endocrine therapy and targeted agents, have contributed to a gradual improvement in 5-year survival rates (Xiong *et al*., 2025). However, the repeated administration of chemotherapeutic agents often leads to diminished treatment efficacy in many patients. Numerous studies suggest that this reduced effectiveness is largely attributable to the development of resistance to chemotherapy drugs (Khan *et al*., 2024).

The pathogenesis of BC is highly complex and remains uncertain (Li *et al*., 2022). Histidine triad nucleotide-binding protein 2 (HINT2) is localized in mitochondria and primarily functions in cellular energy metabolism (Jung *et al*., 2019). Notably, HINT2 expression has been downregulated in various malignant tumors (Li *et al*., 2017, Zhang *et al*., 2024). Although initially identified as a hydrolase, HINT2's mitochondrial localization suggests a broader role in cellular processes, particularly in the regulation of inflammation, an essential function of mitochondria as central hubs of energy metabolism (Wang *et al*., 2025). Previous studies have demonstrated that HINT2 plays a role in activating mitochondrial-associated innate immune and inflammatory responses (Bretes *et al*., 2013). However, few studies have investigated the role of HINT2 in BC. Therefore, further studies are needed to elucidate its role in BC.

The NLRP3 inflammasome, also known as NOD-like receptor protein 3, is a fundamental component of innate immune responses. It facilitates caspase-1 activation, induces pyroptotic cell death and promotes release of pro-inflammatory mediators including but not limited to interleukin-1β (IL-1β) and interleukin-18 (IL-18) (Jo *et al*., 2016). This molecular complex becomes operational following exposure to heterogeneous activators, damage-associated molecular patterns (DAMPs), encompassing pathogen-associated molecular patterns (PAMPs) and endogenous stress indicators. (Ma, 2023). Aberrant NLRP3 functionality demonstrates significant associations with chronic inflammatory conditions, metabolic syndromes and oncogenic processes (Sharma and Kanneganti, 2021). Therefore, we seek the roles of HINT2 and NLRP3 in BC.

Although standard chemotherapeutic and immunotherapeutic regimens can induce complete remission in approximately 50–70% of patients, 30–40% fail to respond or experience relapse following remission, resulting in poor prognosis (Kurdi *et al*., 2023). Albiflorin (Al), a monoterpene glycoside predominantly isolated from the roots of Paeonia lactiflora and related species, has

*Corresponding author: e-mail: cyytt2000@sina.com

attracted considerable research interest owing to its broad-spectrum therapeutic properties (Ou *et al*., 2024, Yang and Yang, 2023). Al has demonstrated a wide spectrum of pharmacological activities, ranging from antioxidant and anti-inflammatory effects (Wang *et al*., 2023, Xu *et al*., 2019, Gao *et al*., 2024). However, its role in BC remains unclear. Therefore, we evaluated the potential effects of Al on BC.

MATERIALS AND METHODS

Reagent

Al (A768918, purity: ≥95%) was purchased from Macklin (Shanghai, China). DMEM medium (#10569010) was purchased from Shanghai Jingkang Bioengineering Co., Ltd. Fetal bovine serum (#10270106) was procured from Shanghai Huicheng Biotechnology Co., Ltd; Liposome 3000 (#L3000015) was obtained from Shanghai Yuanpei Biotechnology Co., Ltd. Penicillin/Streptomycin (#15140122) was procured from Omega Bio Tek, USA. Reverse transcription and real-time PCR kits (#BTN190504) were purchased from Beijing Quanshijin Company. ELISA kits of IL-1β (CSB-E08054m), TNF-α (CSB-E04741m) and IL-6 (CSB-E04639m-IS) were procured from CUSABIO (Wuhan, China). HINT2 (ab220935) antibody was purchased from Abcam Company. NLRP3 (#15101), BcL-2 (#3498), Bax (#2772), Caspase-3 (#9962) were sourced from Cell Signaling Technology Company (USA).

Animals

Twelve 6-week-old female BALB/c-nu mice (6 per group) were procured from the Cavens (Changzhou, China). All experimental procedures involving animals received approval from Research Council and Animal Care and Use Committee of Animal Center of Nanjing Medical University. Mice were housed at 22 ± 2 °C, 55 ± 5 % humidity, 12 h light/12 h dark cycle with free access to food and water. The animal welfare strategy was strictly following 3R principle adherence. Additionally, a daily health-scoring sheet (body-condition score, activity, grooming, respiratory rate) was used; any mouse reaching a cumulative score ≥ 5/15 was immediately euthanized via CO□ asphyxiation followed by cervical dislocation, consistent with AVMA guidelines. After tumor tissue harvest, animals were euthanized without recovery; no animals were kept alive post-experimentation.

MDA-MB-231 cell culture

The proportion of fetal bovine serum in the cell culture medium was set to 7% and the culture dish was placed in a cell culture box at 37°C, containing 6% CO_2 and humidity of 46% for cultivation.

Proteomic analysis of tumor tissue

1. Tumor tissue (TT) and adjacent non-cancerous (PT) tissues were harvested from murine models; liquid nitrogen was used to crush TT.
2. The crushed TT was mixed with TCA-acetone (6-3511, BinGene) and incubated at -20 °C for more than 4 hrs, then dried to obtain protein pellets.
3. The pellets were lysed with 30× (m/v) SDT buffer (SL1029, Coolaber); centrifuged at 14,000 rpm for 5 min at 4 °C, collected the supernatant, filtered through a 0.22 μm membrane and quantified the proteins.
4. The quantified proteins were treated with 5 mmol/L DTT (ST040-1g, Beyotime) at 56 °C for 30 mins for reduction, followed by 11 mmol/L IAA (HY-18569, MCE) at room temperature in the dark for 10–15 mins for alkylation.
5. Dilute the sample to < 2 mmol/L urea (HY-Y0271, MCE); add trypsin (HY-129047, MCE) and incubate overnight, followed by an additional 4 hrs with 1% extra trypsin to digest proteins into peptides.
6. Adding 100 mmol/L DTT, boil for 5 mins, then cool; the sample was loaded into an ultrafiltration tube and centrifuged at 12,500 rpm for 10–15 mins; add IAA buffer, shake at 600 rpm for 1–2 mins and allow to react in the dark for 30 mins, then centrifuge at 12,500 rpm for 15 mins.
7. Wash with 40 mmol/L NH□HCO□ (09830-500g, Sigma-Aldrich) and centrifuge at 12,500 rpm for 15 min; add trypsin buffer, shake and incubate at 37 °C for 16–18 hrs; centrifuge to collect the peptides.
8. Desalt the peptides using a C18 column (75 μm × 25 cm, 1.9 μm, 120 Å, Reprosil-Pur); reconstitute the lyophilized peptides in 0.1% formic acid (5330020050, Sigma-Aldrich) and quantify.
9. Peptides were loaded onto a homemade C18 column (75 μm × 25 cm, 1.9 μm, 120 Å, Reprosil-Pur) installed in an UltiMate 3000 RSLCnano system (Thermo Fisher Scientific, USA).
10. Peptides were separated on an in-house packed C18 column (75 μm × 25 cm, 1.9 μm, 120 Å, Reprosil-Pur) with a binary solvent system: A) 0.1 % formic acid in water and B) 0.1 % formic acid in 80 % acetonitrile, delivered at 300 nL/min.
11. Separating peptides by HPLC and analyze by MS in PASEF mode over 120 mins in positive ion mode (m/z 350–1800); primary MS: 70k resolution, AGC target 3×10^6, IT 50 ms; MS/MS: HCD, 17.5k resolution, 27 eV.
12. Solvent A was 0.1 % formic acid in water; solvent B was 0.1 % formic acid in 80 % acetonitrile (A104440, Aladdin).
13. A 120-mins gradient of 5–30 % B (0–105 mins), 30–50 % B (105–110 mins), 50–95 % B (110–112 mins) and 95 % B (112–120 mins) at 300 nL min□¹ was used for separation.
14. A column blank (0.1 % formic acid) was injected before the first sample and after every 10 injections; a pooled QC sample generated by combining 2 μg of each peptide digest was analysed every 8 runs to monitor system stability.
15. Search MS data using MaxQuant (v1.6.14.0); quantify proteomics data using the LFQ algorithm.Establishment of a BC model in nude mice

All proteomics data are derived from five biologically independent mice per group; each mouse contributed one tumor tissue (TT) and one adjacent non-cancerous (PT) sample processed individually (no pooling) (Meier *et al*., 2018).

MDA-MB-231 human BC cells were implanted subcutaneously into the right flanks of nude mice at a volume of 0.2 mL per mouse. Fourteen days post-inoculation, tumor formation was observed. When the tumor volume reached 80–100 mm^3, xenograft mice were randomly divided into two groups: a model control group and a treatment group receiving Al. The therapeutic group received daily oral gavage of Al (20 mg/kg body weight) once daily for 14 consecutive days.

Establishment of a BC model in-vitro

MDA-MB-231 cells were randomly divided into a model control group and an Al treatment group. Cells in the treatment group were exposed to 20 μM Al for 24 hrs. Following treatment, supernatant from cultured cells was acquired for inflammatory mediator assessment while adherent cells were retrieved for molecular pathway analyses.

Co-immunoprecipitation (Co-IP)

For detection of the endogenous interaction between HINT2 and NLRP3, Co-IP assays were performed using a commercial kit (Pierce™ Co-Immunoprecipitation Kit, #26149, Thermo Fisher Scientific, USA) following the manufacturer's instructions with minor modifications. Briefly, MDA-MB-231 cells or freshly harvested tumor tissues were lysed in ice-cold IP lysis buffer (20 mM Tris-HCl pH 7.4, 150 mM NaCl, 1% NP-40, 1 mM EDTA, 10% glycerol, 1 mM PMSF and 1× protease/phosphatase inhibitor cocktail) for 30 min on ice. After centrifugation at 12,000 × g for 15 mins at 4 °C, the supernatants were collected and protein concentrations were determined using the BCA assay.

A total of 500 μg of protein lysate was pre-cleared with 20 μL of Protein A/G magnetic beads for 1 hr at 4 °C to reduce non-specific binding. The pre-cleared lysates were then incubated overnight at 4 °C with 2 μg of anti-NLRP3 rabbit monoclonal antibody (Cell Signaling Technology, #15101) or control rabbit IgG (Cell Signaling, #3900). Subsequently, 30 μL of fresh Protein A/G magnetic beads were added and incubated for an additional 2 hr at 4 °C with gentle rotation. Immunocomplexes were collected using a magnetic separator and washed five times with ice-cold wash buffer (300 mM NaCl in IP lysis buffer). After the final wash, the beads were resuspended in 2× SDS loading buffer and boiled for 8 min to elute the immunoprecipitated proteins. Samples were then subjected to SDS-PAGE and Western blot analysis using anti-HINT2 antibody (Abcam, ab220935) to detect interacting proteins. Input samples (5% of total lysate) were run in parallel as controls.

Quantitative polymerase chain reaction (qPCR) analysis

Total RNA was extracted from snap-frozen tumor tissues with TRIzol reagent (#15596026, Invitrogen) according to the manufacturer's instructions, followed by DNase I (#EN0521, Thermo Fisher Scientific) digestion. RNA concentration (260/280 ratio 1.9–2.1) was determined with a NanoDrop-2000 spectrophotometer (Thermo Fisher Scientific, USA); integrity (RIN ≥ 7) was verified on 1.2 % agarose gel. RNA was immediately reverse-transcribed using the PrimeScript RT Reagent Kit (#RR037A, Takara) and stored at -80 °C until use. mRNA expression of HINT2 and the endogenous control GAPDH was then quantified by qPCR on a CFX96 system (Bio-Rad). For HINT2, the forward primer was 5′-ACACGTGTACTCTT-3′ and the reverse primer 5′-ATCCTCTCTCGTTCAAGTCT-3′ (206 bp amplicon). GAPDH (113 bp) was amplified with forward primer 5′-ATCCTCTCTCGTTCAGTCT-3′ and reverse primer 5′-AATCCTCTCGTTCAAGTCT-3′.

Tumor weight

After 14 days, the nude mice were euthanized and the tumor tissues were excised in their entirety. Tumor weights were measured using an electronic balance.

Tumor volume

Following model establishment, the length and width of the tumors were measured every 5 days starting from day 0. Volume quantification employed the modified ellipsoid formula: volume = (length × $width^2$) × 1/2 (Jensen *et al*., 2008). On day 14, after the final measurements of tumor dimensions, the nude mice were euthanized via cervical dislocation.

Histological analysis of tumors

Immediately after excision, tumor tissues were fixed in 4% paraformaldehyde and then paraffin-embedded. Serial sections (5 μm thickness) were prepared, dewaxed in xylene and rehydrated through descending ethanol concentrations. Tissue sections were subsequently stained with hematoxylin and eosin and examined under the microscope.

Determination of inflammatory cytokine levels in serum and cell supernatant

Serum specimens and cell culture supernatants underwent analysis for interleukin (IL)-1β, IL-6 and tumor necrosis factor (TNF)-α concentrations using standardized ELISA methodologies according to kit manufacturers' specifications.

Immunohistochemistry

Immunohistochemical staining of tumor tissues was performed using the SP immunohistochemistry kit. Tissue sections were initially rinsed with phosphate-buffered saline (PBS) and then subjected to epitope retrieval by microwave-assisted heating in citrate buffer (20 mins). Endogenous peroxidases were suppressed with 3% H_2O_2 incubation (15 mins). Non-specific protein interactions

were minimized through 20-minute application of normal goat serum. Primary antibody incubation proceeded overnight at 4°C. The following day, sections were equilibrated to 37 °C for 1 hr. Subsequently, biotin-labeled goat anti-rabbit IgG was incubated at 37 °C for 30 mins, followed by incubation with biotin-labeled streptavidin under the same conditions. Finally, chromogenic visualization was performed using 3,3'-diaminobenzidine with a hematoxylin counterstain, followed by neutral resin mounting for light microscopic assessment.

Western blot analysis

Cellular and tissue proteins were solubilized in ice-cold RIPA buffer (#sc-24948, Santa Cruz Biotechnology, CA) supplemented with 1 mM PMSF and 1× protease/phosphatase inhibitor cocktail. After centrifugation (12 000 g, 15 mins, 4 °C), protein concentration in the clarified supernatant was determined with the BCA kit (#23225, Thermo Fisher Scientific, MA) using BSA as standard. Exactly 30 μg of total protein per lane was mixed with 4× Laemmli buffer, heated (95 °C, 5 mins), resolved on 10 % SDS-PAGE and electro-transferred to 0.22 μm PVDF membranes (#ISEQ00010, Merck Millipore). Membranes were blocked with 5 % non-fat dry milk in TBST (25 mM Tris-HCl pH 7.4, 150 mM NaCl, 0.1 % Tween-20) for 1 hr at room temperature, then incubated overnight at 4 °C with the appropriate primary antibodies. Following three 5-mins washes with TBST, membranes were incubated for 2 hrs at room temperature with HRP-conjugated secondary antibodies (31460, Thermo Fisher Scientific, 1:5000). Immunoreactive bands were visualised with ECL Prime substrate (#RPN2232, GE Healthcare, Buckinghamshire, UK) and quantified by densitometry (ImageJ). Target protein signals were normalised to the corresponding GAPDH band (mouse anti-GAPDH 1:10 000, Santa Cruz sc-365062).

Immunofluorescence

To assess NLRP3 expression in MDA-MB-231 cells, 2 × 10□ cells per well were seeded on 12-mm glass coverslips in 24-well plates 24 h before staining. After two PBS rinses, cells were fixed with 4 % paraformaldehyde (P0099-100ml, Beyotime) for 30 min, permeabilized with 0.5 % Triton X-100 (P0096-100ml, Beyotime) for 5 min and blocked with 5 % BSA for 1 h. Coverslips were then incubated overnight at 4 °C with rabbit anti-NLRP3 primary antibody (ab263899, Abcam, 1:500). Following three PBS washes, goat anti-rabbit IgG (H+L) Alexa Fluor® 488 secondary antibody (#A-110081, Thermo Fisher Scientific, 1:500) was applied for 1 h at room temperature. Nuclei were counterstained with DAPI (5 mins) and images were acquired on a fluorescence microscope (Leica Microsystems, Germany).

Molecular docking between HINT2 and Al

Preparation of compound structure

Preliminarily, Al structural coordinates were retrieved through the PubChem bioinformatics platform to establish its molecular topology (Pubchem, 2024). Afterward, import Chem3D software to optimize and minimize energy using the MM2 module. The optimized structure was then saved in SDF format for subsequent use as the ligand in the docking simulations.

Preparation of target protein structure

HINT2 (PDB ID: 5KM9) protein structure was obtained from RCSB database (RCSB, 2026). The protein structure was undergone thorough preprocessing on the Maestro11.9 platform, utilizing Schrodinger's Protein Preparation Wizard. This process included removing crystallization water, adding missing hydrogen atoms, repairing incomplete bond and peptide segment information. Finally, the energy of the protein was minimized and the geometric structure was optimized.

Molecular docking

The Glide module in the Schrödinger Maestro software suite facilitates the complex processing and optimization steps necessary for molecular docking. Specifically, the Protein Preparation Wizard module handles the preprocessing, optimization and constrained minimization of receptor structures using the OPLS3e force field (Roos *et al*., 2019). Simultaneously, the LigPrep module prepares the compound structure according to its default settings.

Once the receptor is prepared, it is imported into the Glide module for screening. The docking site is precisely defined based on specific protein-ligand coordinates (x=-9.54, y=-4.14, z=3.49). To ensure accurate simulations, a docking box of 15 A x 15 A x 15 A is established. The culmination of this process involves executing molecular docking and screening using the Standard Precision (SP) method to rigorously evaluate potential binding interactions.

Screening and analysis of docking results

To elucidate the aggregation-induced luminescence effect of the compound, we first delve into the intricate interaction modes between the compound and the target protein. This analysis reveals various types of interactions between the compound and protein residues, including but not limited to hydrogen bonding, π-π stacking and hydrophobic associations. Subsequently, we leverage the docking score of the compound as a reference point to provide a comprehensive explanation of its aggregation-induced luminescence properties.

Statistical analysis

Data processing was performed with SPSS software (v20.0; IBM, USA). All values are presented as mean ± SD. Before analysis, normality was examined with the Shapir–Wilk test; Core indicators in this study, such as IL-6 concentration, TNF-α concentration and HINT2 protein expression levels, all met the requirements of normal distribution. Homogeneity of variances was confirmed by Levene's test. For comparisons between two groups, independent samples t-tests were applied. All n values in

the manuscript represent independent biological replicates (not technical replicates). For cell experiments, n = 6; for animal experiments, n = 6. Specific n values are clearly indicated in the legend of each figure. The significance criteria are defined as follows: $P < 0.05$ indicates a statistically significant difference and $P < 0.01$ indicates a highly statistically significant difference.

RESULTS

Proteomic analysis

Quantitative proteomic profiling was conducted to delineate protein expression alterations in orthotopic mammary tumors versus control murine specimens. This analysis identified 167 differentially abundant proteins, comprising 121 upregulated and 46 downregulated species. Bioinformatic analysis revealed that HINT2 exhibited the most pronounced change, characterized by significant upregulation. To validate these findings, verification experiments employing qRCR and western blot methodologies consistently demonstrated pronounced HINT2 overexpression in tumor specimens compared to histologically normal adjacent tissues (Fig. 1).

HINT2 and NLRP3 immunoprecipitation and molecular docking

Immunoprecipitation analysis confirmed that HINT2 and NLRP3 endogenously interact to form protein complexes (Fig. 2). Our study evaluated the molecular docking interactions between Al compounds and the HINT2 target protein. Docking results demonstrated a strong binding affinity, with a binding energy of – 7.36 kcal/mol. Using PyMOL 2.1 software (Schrodinger Inc., New York, NY, USA), the docked complex was visualized to elucidate the binding conformation and identify key interacting residues within the protein's binding pocket. Notably, Al was observed to embed deeply within the protein pocket, displaying an optimal fit; these interactions facilitate the stable complex formation between Al and HINT2 (Fig. 3).

Effects of Al on BC in-vivo and in-vitro

In-vivo model

Effects of Al on tumor weight and volume in BC mice

Therapeutic intervention with Al produced a significant reduction in both tumor weight and volumetric dimensions compared with vehicle-treated xenograft models ($P<0.01$), indicating that Al effectively inhibits tumor growth *in-vivo* (Fig. 4A–B).

Effects of Al on histopathological changes in tumor tissue

Histological examination revealed significant tumor-tissue necrosis and inflammatory-cell infiltration in the model group, whereas these pathological changes were significantly ameliorated following Al administration ($P<0.01$, Fig. 4C). Thus, Al improves the histopathological features associated with BC.

Effects of Al on caspase-3, Bax, Bcl-2 in BC mice

Consistent with the pro-apoptotic effect, Al treatment significantly up-regulated the expression of Caspase-3 and Bax and significantly down-regulated the anti-apoptotic protein Bcl-2 relative to the model group (all $P<0.01$, Fig. 4D). These results suggest that Al promotes apoptosis and thereby contributes to the inhibition of BC progression.

Effects of Al on cytokine levels in serum and tumor tissue

Al administration induced a significant decrease in IL-1β, IL-6 and TNF-α concentrations in both serum and tumor tissue compared with the model group ($P<0.01$, Fig. 4E), indicating that Al attenuates the tumor-associated inflammatory micro-environment.

Effects of Al on HINT2/NLRP3 signaling pathway in BC mice

Western blot and immunohistochemistry showed that Al treatment significantly lowered the protein levels of HINT2 and NLRP3 in tumor tissues relative to the model group ($P<0.01$, Fig. 4F–G). These data indicate that Al suppresses the HINT2/NLRP3 signaling axis, which may underlie its anti-tumor activity in BC.

In-vitro model

Effects of Al on cytokine levels in MDA-MB-231 cells

Pharmacological intervention with Al treatment significantly attenuated cytokine levels in MDA-MB-231 cells relative to untreated controls, as demonstrated by significantly diminished IL-6, IL-1β and TNF-α concentrations (Fig. 5A). This indicates an anti-inflammatory effect of Al *in-vitro*.

Effects of Al on Caspase-3, Bax and Bcl-2 expression in MDA-MB-231 cells

Moreover, Caspase-3 and Bax levels were remarkably increased in the Al-treated group, while Bcl-2 expression was notably down-regulated compared to the model group (Fig. 5B). These differential regulations collectively indicate that Al may induce apoptosis by modulating the Bcl-2 family proteins and caspases.

Effects of Al on HINT2/NLRP3 expression in MDA-MB-231 cells

Furthermore, Al treatment elicited significant suppression of the expression of HINT2 and NLRP3 relative to untreated controls, as demonstrated by Western blot analysis and confocal microscopy (Fig. 5C and D). This indicates that Al may inhibit inflammation-related signaling pathways by downregulating these proteins.

Overall, these results suggest that Al exhibits anti-inflammatory and pro-apoptotic effects in MDA-MB-231 cells, potentially through the regulation of cytokine levels, apoptosis-related proteins and inflammation-associated signaling molecules.

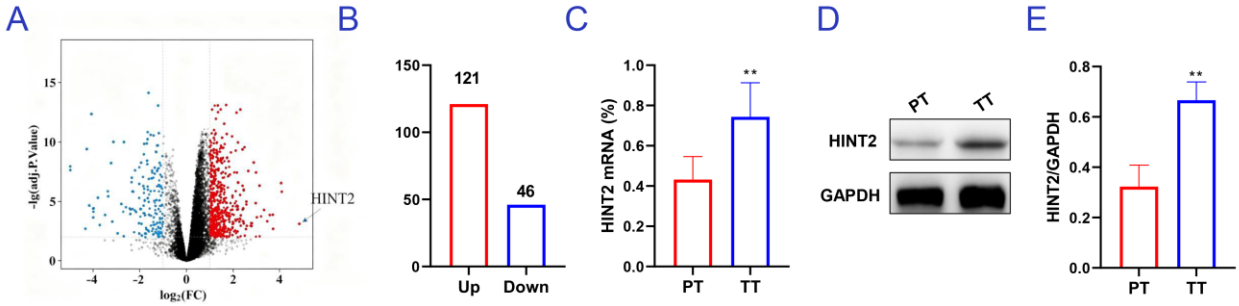

Fig. 1: Proteomic analysis of protein differences in BC mice *(n = 6).*
(A) Differential protein via volcano map analysis; (B) Up and down proteins; (C) The HINT2 mRNA level; (D-E) HINT2 protein level. All the data were presented as mean ± SD. Compared with the control group: $^{**}P<0.01$.

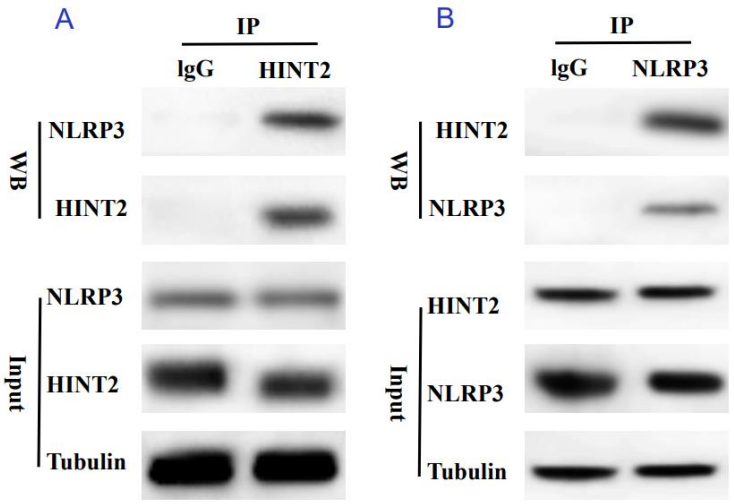

Fig. 2: HINT2 and NLRP3 immunoprecipitation *(n = 3).* (A) Co-immunoprecipitation (Co-IP) assay using anti-HINT2 antibody followed by WB analysis to detect NLRP3; (B) Reciprocal Co-IP assay using anti-NLRP3 antibody followed by WB analysis to detect HINT2. Input samples and Tubulin were used as loading controls to ensure equal protein concentration. HINT2: Histidine triad nucleotide-binding protein 2; NLRP3: NLR family pyrin domain containing 3; Co-IP: Co-immunoprecipitation; WB: Western blot; IgG: Immunoglobulin G.

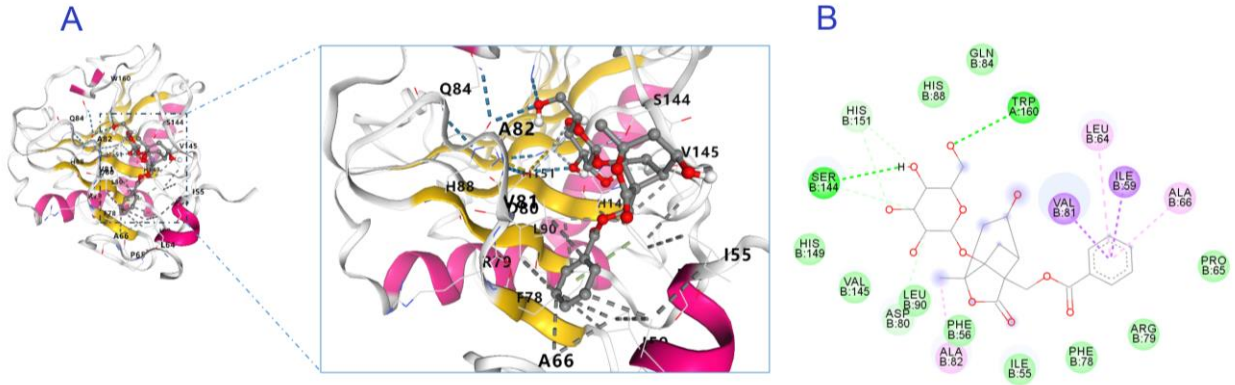

Fig. 3. Molecular docking analysis of the interaction between Albiflorin and HINT2 protein. (A) 3D view of the binding complex between Al and HINT2; (B) 2D diagram illustrating the specific molecular interactions, including hydrogen bonds (green dashed lines) and hydrophobic associations.

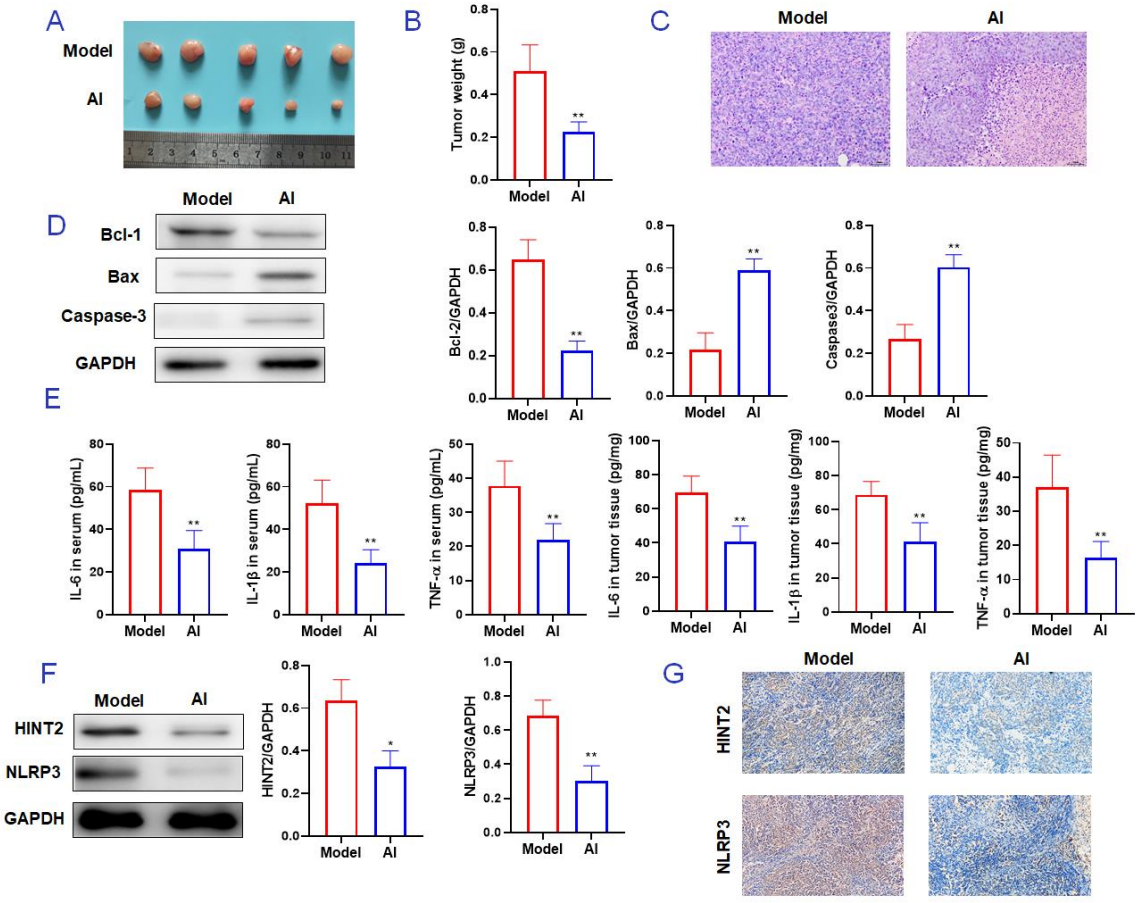

Fig. 4: Effects of Al on BC *in vivo (n = 6).*
(A) Tumor volume; (B) Tumor weight; (C) HE of tumor tissue; (D) Caspase-3, Bax, Bcl-2 in tumor tissues; (E) Cytokine in serum and tumor tissue; (F) The levels of HINT2/NLRP3 signal pathway; (G) Immunohistochemical of HINT2 and NLRP3. All the data was presented as mean ± SD. Compared with model: **P<0.01.

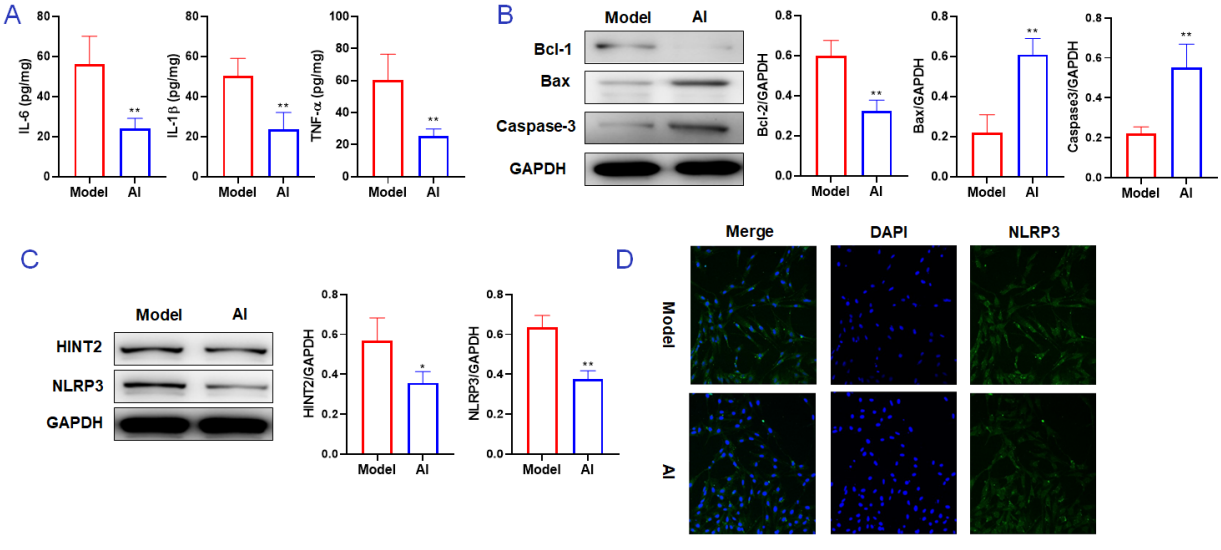

Fig. 5: Effects of Al on BC *in vitro (n = 6).*
(A) Cytokine (B) Caspase-3, Bax, Bcl-2; (C) The levels of HINT2/NLRP3 signal pathway; (D) Immunofluorescence of NLRP3. All the data was presented as mean ± SD. Compared with model: **P<0.01.

DISCUSSION

BC is one of the most prevalent cancers among women worldwide. The annual incidence of BC increases by approximately 1.671 million cases, with around 522,000 deaths attributed to the disease each year (Garcia-Aranda and Redondo, 2017). Despite significant advancements, the pathophysiology and treatment options for BC remain uncertain. Our study investigated the pathophysiological role of HINT2 in BC and assessed the therapeutic effects of Al on the disease. These findings demonstrated that Al exerts its inhibitory effects on BC through the HINT2/NLRP3 signaling pathway. HINT-2, a member of the HINT family within the HIT superfamily, is characterized by the presence of the HIT motif (His-ϕ-His-His-ϕ-ϕ, where ϕ represents a hydrophobic amino acid). Previous studies have reported decreased HINT2 expression in various malignancies (Zhou *et al*., 2019). In colorectal cancer cell, the upregulation of HINT2 could reduce colon cancer cell prognosis through mitochondrial damage by polysaccharide of L. casei SB27 (Di *et al*., 2023). Unlike these findings, we observed a notably increased expression of HINT2 in BC tissues. Considering HINT2's mitochondrial localization and its established role in energy metabolism, we hypothesized that HINT2 may modulate cytokine secretion during acute inflammation by influencing the inflammatory response. Our findings demonstrated significantly elevated HINT2 levels in tumor tissues, implicating a potential regulatory role in inflammatory cytokine production. Notably, treatment with Al significantly reduced HINT2 expression in tumor tissues. Furthermore, coimmunoprecipitation assays revealed a physical interaction between HINT2 and NLRP3; moreover, HINT2 was found to significantly activate NLRP3. Under BC stimulation, HINT2 and NLRP3 levels were significantly upregulated in tumor tissues, whereas Al treatment significantly suppressed their expression. Previous studies implicated inflammatory factors as pivotal drivers in BC pathogenesis (Zahid *et al*., 2016). Current findings revealed pronounced upregulation of IL-1β, IL-6 and TNF-α in BC tissues (Cruceriu *et al*., 2020, Avalle *et al*., 2022, Tunali *et al*., 2023). However, administration of Al significantly reduced the expression of these cytokines. Notably, HINT2 knockout significantly reversed these elevations *in-vivo* and *in-vitro*. Reciprocally, elevated inflammatory mediators activate NLRP3 signaling to propagate inflammatory responses (Li *et al*., 2023). We demonstrate HINT2 inhibition substantially downregulated NLRP3 expression, mirroring the NLRP3 suppression observed following Al exposure. In conclusion, HINT2 represents a significant biomarker in BC and Al exerts its inhibitory effects on BC via modulation of the HINT2/NLRP3 signaling pathway. These findings offer a novel therapeutic target and a potential strategy for the clinical management of BC.

Acknowledgements
None.

Author's contributions
HYP and CYY: Conceived and designed the experiments; HYP, LC and CYY: Performed the experiments; HYP, LC and CYY: Analyzed the data and prepared the figures. All authors contributed to the article and read and approved the final version of the manuscript.

Funding
There was no funding.

Data availability statement
The data underlying this article are available on reasonable request to the corresponding author.

Ethical approval
The experimental procedures carried out in the present study were approved by the Animal Experiment Ethics Committee of The Affiliated Jiangning Hospital of Nanjing Medical University (240076451). This study was performed in adherence with the ARRIVE guidelines. See supplementary file for the ARRIVE checklist.

Conflict of interests
The authors declare no conflict of interest.

REFERENCES

Avalle L, Raggi L, Monteleone E, Savino A, Viavattene D, Statello L, Camperi A, Stabile SA, Salemme V, De Marzo N, Marino F, Guglielmi C, Lobascio A, Zanini C, Forni M, Incarnato D, Defilippi P, Oliviero S and Poli V (2022). STAT3 induces breast cancer growth via ANGPTL4, MMP13 and STC1 secretion by cancer associated fibroblasts. *Oncogene.,* **41**(10): 1456-1467.

Bretes E, Wojdyła-Mamon AM, Kowalska J, Jemielity J, Kaczmarek R, Baraniak J and Guranowski A (2013). Hint2, the mitochondrial nucleoside 5'-phosphoramidate hydrolase; properties of the homogeneous protein from sheep (Ovis aries) liver. *Acta Biochim Pol.,* **60**(2): 249-54.

Cruceriu D, Baldasici O, Balacescu O and Berindan-Neagoe I (2020). The dual role of tumor necrosis factor-alpha (TNF-α) in breast cancer: Molecular insights and therapeutic approaches. *Cell Oncol (Dordr).,* **43**(1): 1-18.

Di W, Li X and Yang Q (2023). Polysaccharide of Lactobacillus casei SB27 reduced colon cancer cell prognosis through mitochondrial damage by upregulation of HINT2. *Asia Pac J Clin Oncol.,* **19**(5): e248-e257.

Gao L, Fu W, Liu Y, Fan L, Liu S and Zhang N (2024). Albiflorin inhibits advanced glycation end products-induced ROS and MMP-1 expression in gingival fibroblasts. *Curr Stem Cell Res Ther.*, **20**(4): 434-440.

García-Aranda M and Redondo, M (2017). Protein kinase targets in breast cancer. *Int J Mol Sc.i.,* **18**(12): 2543.

Jensen MM, Jørgensen JT, Binderup T and Kjaer A (2008).

Tumor volume in subcutaneous mouse xenografts measured by microCT is more accurate and reproducible than determined by 18F-FDG-microPET or external caliper. *BMC Med Imaging.,* **8**: 16.

Jo EK, Kim JK, Shin DM and Sasakawa C (2016). Molecular mechanisms regulating NLRP3 inflammasome activation. *Cell Mol Immunol.,* **13**(2): 148-159.

Jung A, Yun JS, Kim S, Kim SR, Shin M, Cho DH, Choi KS and Chang JH (2019). Crystal structure of histidine triad nucleotide-binding protein from the pathogenic fungus *Candida albicans*. *Mol Cells.,* **42**(1): 56-66.

Khan MM, Yalamarty S SK, Rajmalani BA, Filipczak N and Torchilin VP (2024). Recent strategies to overcome breast cancer resistance. *Crit Rev Oncol Hematol.,* **197**: 104351.

Kim S, Chen J, Cheng T, Gindulyte A, He J, He S, Li Q, Shoemaker Benjamin A, Thiessen Paul A, Yu B, Zaslavsky L, Zhang, J and Bolton Evan E (2025). PubChem 2025 update. *Nucleic Acids Research*., **53**: D1516–D1525.

Kurdi M, Mulla N, Malibary H, Bamaga AK, Fadul MM, Faizo E, Hakamy S and Baeesa S (2023). Immune microenvironment of medulloblastoma: The association between its molecular subgroups and potential targeted immunotherapeutic receptors. *World J Clin Oncol.,* **14**(3): 117-130.

Li W, Cai S, Wang L, Yang C, Zhou B and Wang H (2017). HINT2 downregulation promotes colorectal carcinoma migration and metastasis. *Oncotarget.,* **8**(8): 13521-13531.

Li Y, Wang M, Yang S, Kuang L, Tao X, Yang J, Zhao W and Zhang J (2022). Intratumoral heterogeneity contributes to the chemotherapy prognosis of breast cancer. *J Cancer Res Ther.,* **18**(5): 1268-1275.

Li Z, Pan H, Yang J, Chen D, Wang Y, Zhang H and Cheng Y (2023). Xuanfei Baidu formula alleviates impaired mitochondrial dynamics and activated NLRP3 inflammasome by repressing NF-κB and MAPK pathways in LPS-induced ALI and inflammation models. *Phytomedicine.,* **108**: 154545.

Ma Q (2023). Pharmacological inhibition of the NLRP3 inflammasome: Structure, molecular activation and inhibitor-NLRP3 Interaction. *Pharmacol Rev.,* **75**(3): 487-520.

Meier F, Brunner AD, Koch S, Koch H, Lubeck M, Krause M, Goedecke N, Decker J, Kosinski T, Park MA, Bache N, Hoerning O, Cox J, Räther O and Mann M (2018). Online parallel accumulation-serial fragmentation (PASEF) with a novel trapped Ion mobility mass Spectrometer. *Mol Cell Proteomics.,* **17**(12): 2534-2545.

Ou Z, Li P, Wu L, Wu Y, Qin L, Fang L, Xu H, Pei K and Chen J (2024). Albiflorin alleviates neuroinflammation of rats after MCAO via PGK1/Nrf2/HO-1 signaling pathway. *Int Immunopharmacol.,* **137**: 112439.

Pubchem. (2026). *Albiflorin* [Online]. Available: https://pubchem.ncbi.nlm.nih.gov/compound/24868421 [Accessed 23/01/26 2026]

Roos K, Wu C, Damm W, Reboul M, Stevenson JM, Lu C, Dahlgren MK, Mondal S, Chen W, Wang L, Abel R, Friesner RA and Harder ED (2019). OPLS3e: Extending force field coverage for drug-like small molecules. *J Chem Theory Comput.,* **15**(3): 1863-1874.

Sharma BR and Kanneganti TD (2021). NLRP3 inflammasome in cancer and metabolic diseases. *Nat Immunol.,* **22**(5): 550-559.

Tunali G, Yanik H, Ozturk SC, Demirkol-Canli S, Efthymiou G, Yilmaz KB, Van Obberghen-Schilling E and Esendagli G (2023). A positive feedback loop driven by fibronectin and IL-1β sustains the inflammatory microenvironment in breast cancer. *Breast Cancer Res.,* **25**(1): 27.

RCSB. (2026). *Human histidine triad nucleotide binding protein 2 (hHint2) adenosine complex* [Online]. Availabe: https://www.rcsb.org/structure/5KM9 [Accessed 02/15/26 2026]

Wang Q, Guo Y, Chen S, Liu Z, Wang X, Huang H, Shen QE, Yang L, Li M, Li Y, Yu C and Xu C (2025). Histidine triad nucleotide-binding protein 2 attenuates metabolic dysfunction-associated steatotic liver disease through NAD(+)-dependent sirtuin-3 activation. *Exp Mol Med.*, **57**(5): 990-1004.

Wang X, Su L, Tan J, Ding T and Yue Y (2023). Albiflorin alleviates DSS-induced ulcerative colitis in mice by reducing inflammation and oxidative stress. *Iran J Basic Med Sci.,* **26**(1): 48-56.

Xiong X, Zheng LW, Ding Y, Chen YF, Cai YW, Wang LP, Huang L, Liu CC, Shao ZM and Yu KD (2025). Breast cancer: Pathogenesis and treatments. *Signal Transduct Target Ther.,* **10**(1): 49.

Xu YJ, Mei Y, Shi XQ, Zhang YF, Wang XY, Guan L, Wang Q and Pan HF (2019). Albiflorin ameliorates memory deficits in APP/PS1 transgenic mice via ameliorating mitochondrial dysfunction. *Brain Res.,* **1719**: 113-123.

Yang R and Yang Y (2023). Albiflorin attenuates high glucose-induced endothelial apoptosis via suppressing PARP1/NF-κB signaling pathway. *Inflamm Res.,* **72**(1): 159-169.

Zahid H, Simpson ER and Brown KA (2016). Inflammation, dysregulated metabolism and aromatase in obesity and breast cancer. *Curr Opin Pharmacol.,* **31**: 90-96.

Zhang N, Zhou ZY, Meng YY, Liao HH, Mou SQ, Lin Z, Yan H, Chen S and Tang QZ (2024). HINT2 protects against pressure overload-induced cardiac remodelling through mitochondrial pathways. *J Cell Mol Med.,* **28**(8): e18276.

Zhou DK, Qian XH, Cheng J, Chen LH and Wang WL (2019). Clinical significance of down-regulated HINT2 in hepatocellular carcinoma. *Medicine (Baltimore).,* **98**(48): e17815.